J Solid State Electrochem (2012) 16:3573–3580
DOI 10.1007/s10008-012-1785-5

ORIGINAL PAPER

Temperature stable supercapacitors based on ionic liquid and mixed functionalized carbon nanomaterials

R. S. Borges · H. Ribeiro · R. L. Lavall · G. G. Silva

Received: 23 February 2012 / Revised: 20 May 2012 / Accepted: 23 May 2012 / Published online: 9 June 2012

Abstract The ionic liquid 1-butyl-2,3-dimethylimidazolium bis(trifluoromethylsulfonyl)imide (BDMIM-TFSI) showed a conductivity of 1.65 mS cm^{-1} and an electrochemical stability window of 4.4 V at room temperature. Two types of electrodes based on carbon nanomaterials were prepared: (1) with alternating layers of two oppositely charged functionalized double-walled carbon nanotubes (DWCNTs) and (2) with the functionalized DWCNTs and graphene oxide nanoplatelets. The electrodes presented a porous morphology and a connected pathway between the carbon nanotubes and graphene oxide platelets. Electrochemical capacitors based on the carbon nanomaterials and BDMIM-TFSI were produced in a stacking configuration and were characterized at 25 °C, 60 °C, and 100 °C. The supercapacitors with electrodes based on the three alternating layers of two oppositely charged DWCNTs and graphene oxide presented higher values of capacitance, which were attributed to a morphology favorable to providing ionic access to the carbonaceous surface. Box-like voltammetric curves were used to calculate the capacitance in a 4-V potential window at 100 °C.

Keywords 1-Butyl-2,3-dimethylimidazolium bis(trifluoromethylsulfonyl)imide · Double-walled carbon nanotubes · Graphene oxide nanoplatelets · Electrochemical capacitors

R. S. Borges · H. Ribeiro · R. L. Lavall · G. G. Silva (✉)
Departamento de Química, Instituto de Ciências Exatas,
Universidade Federal de Minas Gerais,
31270-901, Belo Horizonte, Brazil
e-mail: glaura@qui.ufmg.br

Introduction

The current electric double layer capacitors or supercapacitors can operate at very high charge–discharge rates and can have lifetimes of over a million cycles [1, 2]. However, some specific problems must be overcome to ensure broader applications of these devices. Some of the limitations are as follows: (1) lower energy storage than batteries [1–3], (2) failure to filter voltage ripple [4], and (3) instability in applications at temperatures of 60 °C and higher [5, 6]. The use of ionic liquids as an electrolyte can contribute to the safer use of supercapacitors for harvesting energy; for instance, when vehicles must be stopped, their operation involves temperatures of at least 60 °C.

Ionic liquids of cyclic cations exhibit unique properties including inflammability, negligible vapor pressure, high thermal and chemical stability, and conductivity values higher than 1 mS cm^{-1} [7–11]. These ionic liquids have been used in many electrochemical devices such as lithium batteries [7, 12, 13], capacitors [3, 5, 7, 14], solar cells, fuel cells, and others [7]. The ionic liquid 1-butyl-2,3-dimethylimidazolium bis(trifluoromethylsulfonyl)imide (BDMIM-TFSI) and other similar ionic liquids have been studied by groups interested in their basic physicochemical properties [8, 15, 16] and their applications in batteries [13] and supercapacitors [5].

Carbonaceous materials, and high surface area amorphous carbon in particular, are widely used as electrodes in supercapacitors [6, 17, 18]. Ionic liquids have larger anions and cations than aqueous electrolytes, and the size of the ionic species should be paired with the porosity range of the carbonaceous at the electrodes to be able to take advantage of the double layer capacitance [19–21].

Carbon nanotubes (CNT) have been extensively investigated for applications in electrochemical capacitors [22–26].

Nanotubes can have high electrical conductance along the tubes and can have a morphology tailored to allow a suitable range of porosity [25]. Recently, graphene and its derivates [3, 4, 27–31] have been raised as promising candidates for use in supercapacitor electrodes. Graphene oxide nanoplatelets are one of the materials that can be solution processed to prepare electrodes.

This work presents an investigation of supercapacitors based on an ionic liquid with an imidazolium cation and two different types of electrodes. The morphological and electrochemical characteristics of the electrodes based on functionalized double-walled carbon nanotubes (DWCNT) and a mixture of DWCNT with graphene oxide nanosheets (GON) (DWCNT_GON) were studied. The mixed carbonaceous electrodes may present changes in the morphology of the carbonaceous packing because the 1D and 2D nanomaterials adopt specific configurations under deposition differently than those produced by the self-arrangement of nanotubes alone. The primary goal is to produce a supercapacitor that works with increased safety and shows improved performance at higher temperatures.

Experimental

Materials and sample preparation

The commercial ionic liquid 1-butyl-2,3-dimethylimidazolium bis(trifluoromethylsulfonyl)imide (Iolitec—Germany) with 99 % purity and water content of less than 100 ppm, according to the supplier, was used as received. Handling of the ionic liquid was carried out in a glove bag under a nitrogen atmosphere.

The commercial double-walled carbon nanotubes (Nanocyl—Belgium) were synthesized by chemical vapor deposition and functionalized with carboxylic (DWCNT–COOH) and amine groups (DWCNT–NH_2) as stated by the supplier. The extent of modification of these carbon nanotubes was characterized by thermogravimetric analysis, and the results will be discussed later in "Functionalized double-walled carbon nanotubes and graphene oxide nanosheets" section. In a previous work from our group, we reported a detailed characterization of the DWCNT–COOH sample [32]. These carbon nanotubes were used to prepare the electrodes for use in electrochemical capacitors.

Commercially available expanded graphite (Nacional de Grafite—Brazil) was used to produce oxidized graphene nanosheets synthesized by modified Hummers method [33, 34]. Concentrated sulfuric acid was added to the expanded graphite power with sodium nitrate in an ice bath followed by the gradual addition of $KMnO_4$. The mixture was stirred for 4 h and diluted with de-ionized (DI) water. Graphite oxide was obtained after addition of H_2O_2. The graphite oxide was re-dispersed in DI water and exfoliated to generate graphene oxide nanosheets by ultrasonication. The sample was filtered and washed with a diluted acid solution to remove metal ions and then washed with DI water until its pH reached 7. Finally, the graphene oxide nanoplatelets were dried at 100 °C over 12 h. All reagents were used as received. As with the carbon nanotubes, GON was used to prepare electrodes for use in electrochemical capacitors.

The carbon nanotubes electrodes were prepared by dispersing each type of functionalized DWCNT in distilled water using a low-power ultrasonic bath for 4 h until stable dispersions were obtained. Then, the dispersions were deposited onto stainless steel substrates by drop casting, alternating a coating of DWCNT–NH_2 with a coating of DWCNT–COOH. Samples with 20 coatings, 10 of each nanotube type, were dried at 100 °C. The use of alternating layers of –NH_2– and –COOH–modified DWCNTs allows for improved electrode quality because these functional groups create CNT interactions based on opposite charges [35]. The electrodes based on alternating layers of functionalized DWCNTs are referred to as DWCNT electrodes for conciseness.

The previously described method was also used to prepare mixed electrodes; however, in this case, the electrodes were prepared with three different layers: DWCNT–NH_2, DWCNT–COOH, and GON. The samples were prepared with 10 trilayers and dried at 100 °C. The electrodes exhibited a thickness in the micrometer range.

Electrochemical capacitors were prepared in a stacked configuration with two carbon electrodes (in contact with stainless steel current collectors) with an ionic liquid layer in-between as an electrolyte. A paper disk separator was used to support the ionic liquid.

Measurements

Thermal characterization of the ionic liquid was obtained by thermogravimetric measurements (TG) and differential scanning calorimetry (DSC). Thermogravimetric measurements were performed with a TA Instruments SDT 2960 in nitrogen atmosphere at a heating rate of 10 °C min^{-1}. DSC measurements were carried out with a TA Instruments 2920 DSC. The sample was first heated from room temperature to 150 °C, then cooled to −150 °C, and heated to a temperature of 150 °C at a heating rate of 5 °C min^{-1} under a helium atmosphere. Approximately 15 mg of ionic liquid was used in TG and DSC measurements.

Electrical measurements were performed with an AUTOLAB PGSTAT 30 ECOCHEMIE frequency analyzer. The impedance measurements were conducted using a frequency range of 0.5 MHz to 0.1 Hz at 0 V with amplitude of 10 mV. Cyclic voltammetry experiments were performed in different potential windows ranging from 0.5 V to 5 V with a scan

rate of 50 mV s^{-1}. A silver wire was used as a pseudo-reference electrode for the ionic liquid characterization.

The quality of the carbon nanotubes and graphene oxide nanoplatelets was studied by transmission electron microscopy (TEM) and thermogravimetric measurements. TEM images were obtained on a FEI TECNAI® G2 with a thermo-ionic gun at 200 kV. The TEM sample preparation was conducted by dispersing the carbon nanotubes in isopropyl alcohol and graphene oxide nanosheets in THF using a low-power ultrasonic bath. Drops of the dispersions were deposited onto holey carbon-coated copper grids. TG measurements were performed with a TA Instruments SDT 2960 in an air atmosphere at a heating rate of 5 °C min^{-1}.

The morphology of the carbon-based electrodes was studied by scanning electron microscopy (SEM). Images were obtained with a FEI QUANTA 200® scanning electron microscope in a low-vacuum mode, without any cover over the samples.

Electrochemical capacitors were studied by impedance spectroscopy, cyclic voltammetry (CV), and galvanostatic charge–discharge tests. All measurements were carried out with an AUTOLAB PGSTAT 30 ECOCHEMIE frequency analyzer. The impedance measurements were conducted using a frequency range of 1 MHz to 0.1 Hz at 0 V with an amplitude of 10 mV. Cyclic voltammetry experiments were performed in potential windows varying between 1 V and 4 V with scan rate of 100 mV s^{-1}. Impedance and cyclic voltammetry were performed at 25 °C, 60 °C, and 100 °C. Galvanostatic charge–discharge curves were obtained by applying a current density of 1 mA cm^{-2} between two different voltage ranges: 0–2 V or 0–3 V. Measurements were carried out at 60 °C over 2,000 cycles.

Results and discussion

The results will be presented in three parts: the characterization of the ionic liquid, the characterization of the different carbon nanomaterials and the electrodes prepared with them, and, finally, the investigation of electrochemical features of the supercapacitors.

Ionic liquid

Thermogravimetric measurements for 1-butyl-2,3-dimethylimidazolium bis(trifluoromethylsulfonyl)imide (BDMIM-TFSI) indicated high thermal stability with a maximum value of derivative mass loss (DTG) at 484 °C. The onset of thermal decomposition was observed at 355 °C. Previous work reported similar ranges in the ionic liquid thermal decomposition [13, 36]. DSC results showed that the ionic liquid BDMIM-TFSI presented one glass transition (T_g) at −79 °C. Nadherna et al. [13] determined T_g for BDMIM-TFSI to be −81 °C, which can be considered equivalent due to differences in experimental conditions.

Impedance spectroscopy was applied to investigate the ionic liquid conductivity in the range of 25 °C to 110 °C as shown in Fig. 1a. The Arrhenius plot in Fig. 1a shows a quasi-linear increase in conductivity values with an increase of temperature. A conductivity value of 1.65 mS cm^{-1} was observed for BDMIM at room temperature. The value of conductivity reached 7.5 mS cm^{-1} at 100 °C. Previous reports [11, 13] obtained an identical value for the conductivity at room temperature, or 20 °C. However, Nadherna et al. [13] observed a more pronounced increase in the conductivity as a function of temperature than the trend showed in Fig. 1a and obtained by Bazito et al. [11].

Cyclic voltammetry measurements (Fig. 1b) were used to determine the electrochemical stability of the ionic liquid. The ionic liquid has a water content of less than 100 ppm, according to supplier. BDMIM-TFSI showed an electrochemical stability window value of 4.4 V. This result is in general agreement with other studies regarding ionic liquids that are reported in literature [5, 8, 10, 11, 13].

Functionalized double-walled carbon nanotubes and graphene oxide nanosheets

The thermogravimetric curves for carbon nanotubes and graphene oxide nanosheets (Fig. 2) indicate high carbon purity for all samples: the residues at 900 °C, associated with metal oxide from the catalysts, show only 3 mass% for DWCNT–COOH and GON and 9 mass% for DWCNT–NH_2. The profiles in Fig. 2 present two stages of decomposition in air atmosphere. The first stage is associated with the functional groups and is observed from ~100 °C up to 300 °C for all samples. The amounts of the functional groups that decompose were as follows: 8 mass% for DWCNT–COOH, 2 mass% for DWCNT–NH_2, and 12 mass% for GON. The second stage corresponds to the thermo-oxidation of carbon materials, and this stage shows a maximum rate of reaction at 500 °C and 670 °C for carbon nanotubes and graphene nanoplatelets, respectively.

Figure 3 shows typical images from transmission electron microscopy in which it is possible to observe the high quality of the nanotubes (Fig. 3a, b) even after chemical modifications. This characteristic is very important to application of the materials in electrochemical devices because it is associated with high conductivity. Figure 3a and b also shows tubes of differing diameters; however, the diameter values are always lower than 5 nm. TEM images of graphene oxide nanoplatelets are presented in Fig. 3c and d. Figure 3c shows the overview of one transparent and corrugated sheet. Figure 3d shows a GON region on edge with seven layers. This image is typical of the GON obtained using our preparation conditions. Platelets of less than 5 nm

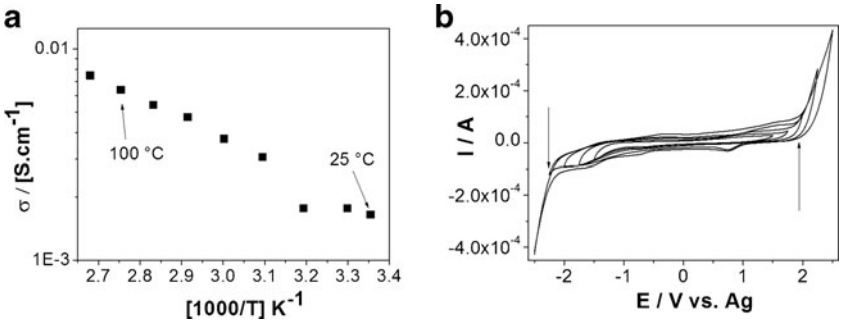

Fig. 1 **a** Arrhenius plot for 1-butyl-2,3-dimethylimidazolium bis(trifluoromethylsulfonyl)imide (BDMIM). **b** Cyclic voltammograms for BDMIM with an increased potential window with respect to Ag (pseudo-reference)

were frequently observed. This thickness of GON is also the result typically obtained by other groups [27] employing similar expanded graphite samples and exfoliation methods.

The carbon nanotubes electrodes were prepared by drop casting alternating layers of the carbon nanomaterials DWCNT–NH_2 and DWCNT–COOH. This method is easy to apply and was employed to allow interactions between layers with the functional surface groups, –NH_2 and –COOH. The carbon nanotube electrodes were prepared as shown in Fig. 4a, with alternating stacked layers of functionalized nanotubes. These electrodes are referred to as DWCNTs to be concise and to emphasize that these electrodes were made using only functionalized, double-walled carbon nanotubes. Mixed electrodes based on carbon nanotubes and graphene oxide nanoplatelets were prepared by deposition of layers in the following order: DWCNT–NH_2, DWCNT–COOH, and then GON. Those mixed electrodes were named DWCNT_GON (Fig. 4b). The surface morphology and quality of the electrodes were analyzed by scanning electron microscopy.

Figure 5 shows SEM images for the surfaces of the two types of electrodes with distinct magnifications. The electrodes based in functionalized carbon nanotubes (DWCNT), Fig. 5a–b, exhibit a carbon nanotube porous network in which bundles and single tubes overlap. The network completely covers the surface with a rough texture that produces great contact with electrolyte. Furthermore, this porous morphology helps large size ions to improve infiltration through the electrodes. This morphology is similar to the electrodes prepared with DWCNT–COOH in our previous work [32].

The second type of electrode, based in functionalized carbon nanotubes and graphene oxide nanosheets (DWCNT_GON), is shown in Fig. 5c–d. It is interesting to note that the GON connected some agglomerates of

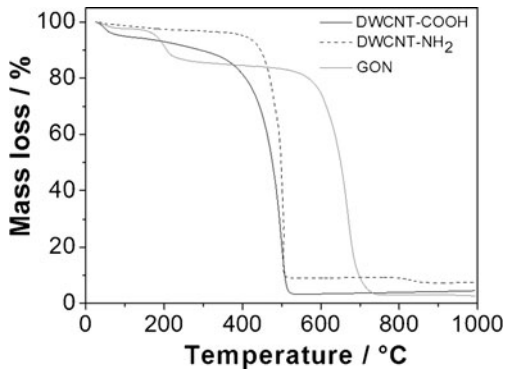

Fig. 2 Thermogravimetric curves for DWCNT–NH_2, DWCNT–COOH, and GON in air

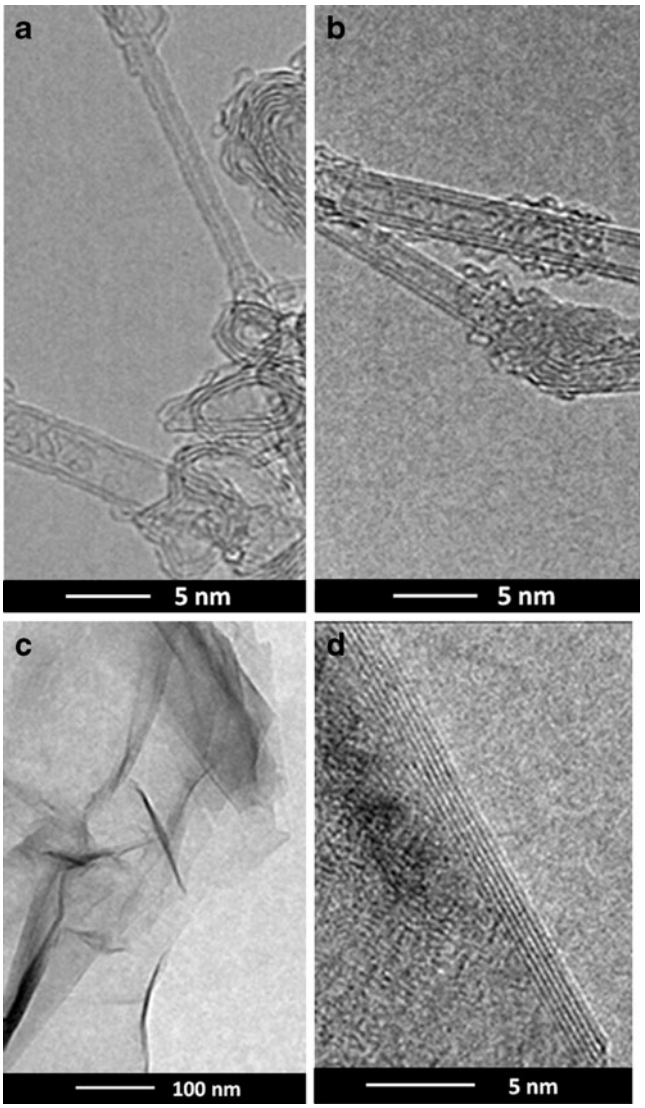

Fig. 3 Transmission electron microscopy with distinct magnification: **a** DWCNT–NH_2, **b** DWCNT–COOH, **c** and **d** GON

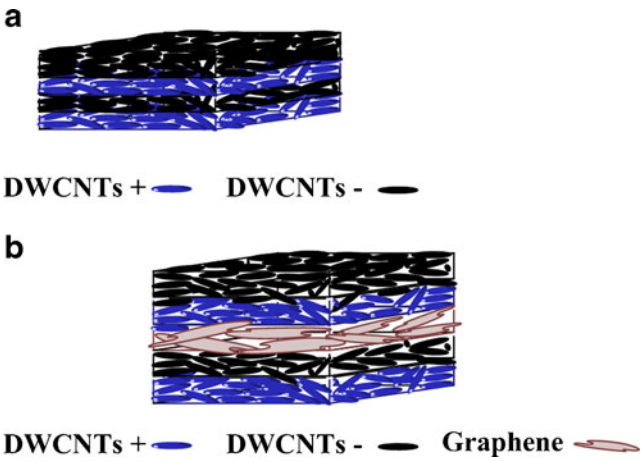

Fig. 4 Scheme for the stacking of carbonaceous layers in the two types of electrodes produced by dropping: **a** DWCNT (DWCNT–NH_2 and DWCNT–COOH alternating layers), the final electrode was prepared with 20 times the bilayer; **b** DWCNT_GON (also with alternating layers of functionalized DWCNT and a third layer of GON), the final electrode was prepared with 10 times the trilayer

carbon nanotubes and can operate as a support for the next layers of carbon nanotubes as shown in Fig. 5d. Moreover, in electrodes based on DWCNT_GON, it is possible to observe some nanosheets of large areas. The surface morphologies are slightly different when comparing DWCNT electrodes (with alternating layers of functionalized nanotubes) and DWCNT_GON electrodes because the latter has regions with a smoother, less porous, graphene oxide surface. Furthermore, packing carbonaceous nanomaterials with different morphologies (e.g., tubes and platelets) may allow for a larger volume of open space in the electrode bulk, as proposed in Fig. 4b, in comparison to the DWCNT electrode.

The electrochemical study showed that some differences correlated to the morphologies were observed in the behavior of the device as discussed in the following section.

Electrochemical capacitors

The complete cell is composed of two electrodes of carbon nanomaterials separated by one layer of ionic liquid (BDMIM–TFSI) supported by a paper separator. Two different capacitors were produced; one with DWCNT–based electrodes and one with DWCNT_GON-based electrodes, both using functionalized nanotubes. The electrochemical behavior of the different supercapacitors was studied by impedance spectroscopy and cyclic voltammetry measurements.

Figure 6a shows Nyquist plots for the two capacitors in which it is possible to observe typical electrochemical capacitor behavior based on porous electrodes with large areas of contact. In this case, a semicircle was obtained in the high frequency region, followed by two linear regions at intermediate and low frequencies with slopes of approximately 45° and 90°, respectively [37, 38]. The equivalent circuit

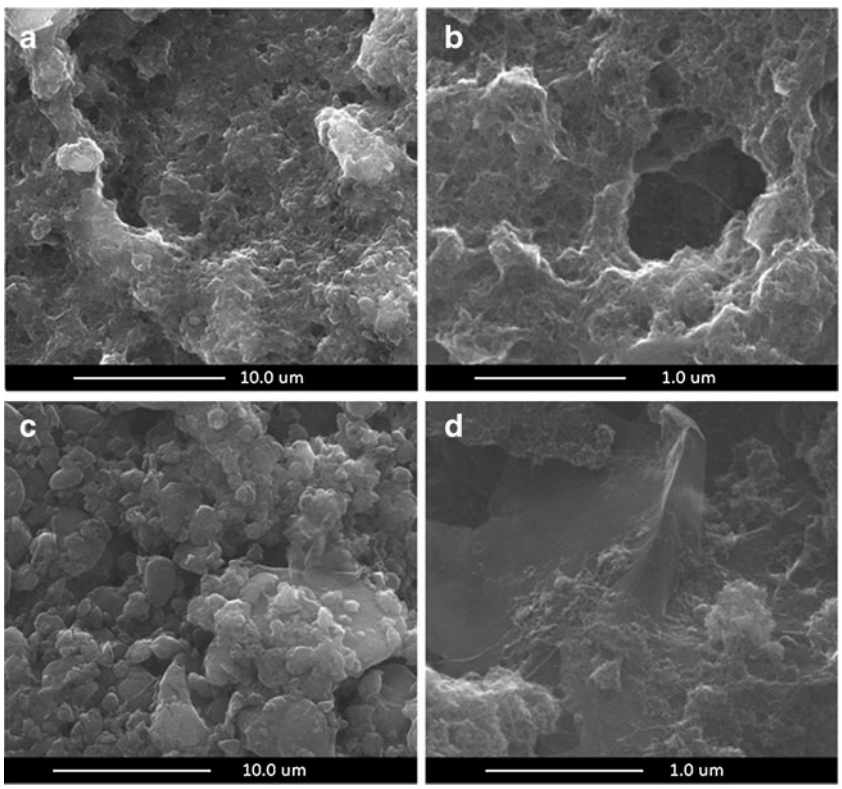

Fig. 5 Scanning electron microscopy with distinct magnification for the surface of the electrodes based on **a**, **b** DWCNT (DWCNT–NH_2 and DWCNT–COOH alternated layers) and **c**, **d** DWCNT_GON (also with alternating layers of functionalized DWCNT and a third layer of GON)

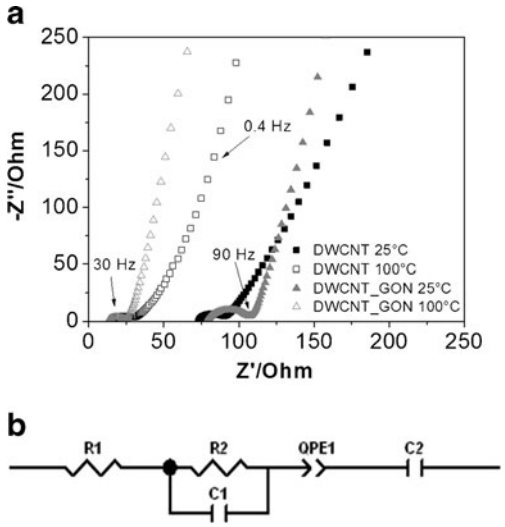

Fig. 6 Electrochemical behavior of complete cell using current collector| carbon electrode| ionic liquid| carbon electrode| current collector configuration: **a** Nyquist plots for supercapacitors at different temperatures, **b** equivalent circuit proposed for the impedance interpretation. (DWCNT means layers of alternated functionalized nanotubes)

proposed for the complete cell is shown in Fig. 6b. The circuit has two resistors connected in series (R1 and R2); the second one is connected in parallel with one capacitor (C1), followed by one constant phase element (CPE1) and a second capacitor (C2).

The two high frequency resistors (R1 and R2) present values that vary strongly over the temperature range studied (Fig. 6); therefore, they may be assigned to ionic liquid charge transport through the carbon electrodes and separator. A high frequency capacitance (C1) can be attributed to polarization involving the ionic liquid. The constant phase element (CPE1) is used to describe the data with a slope of approximately 45° in the intermediate frequency range. This behavior represents the Warburg impedance of the system, present in porous electrodes. The equivalent circuit that allows a good fit to the impedance results has a low frequency capacitance (C2) that is associated with polarization between the carbon electrodes and the ions in the ionic liquids.

The Nyquist plots in Fig. 6a show that the capacitors with DWCNT electrodes (alternated layers of functionalized nanotubes) or with mixed DWCNT_GON presented similar behavior, making all components in the equivalent electric circuit (Fig. 6b) necessary to fit their impedance results. The graphene oxide nanosheets appear to make a small contribution to change the capacitance value; an increase from 37.9 $F g^{-1}$ to 39.1 $F g^{-1}$ at 100 °C was observed as shown in Table 1. This result suggests that carbon nanotubes are primarily responsible for electric double layer formation at the carbon electrode/ionic liquid interface.

Moreover, it should be considered that the GON is not a highly conductive material because a high content of oxygenated functions [27] disturbs its electrical behavior. Therefore, the higher capacitance observed in the mix electrode is probably the result of a change in morphology. The nanoplatelets may have a contribution that extends the availability of the carbonaceous surface to a double layer formation. This contribution was attributed to looser packing of the carbonaceous, as shown in Fig. 4b.

In support of this discussion, it can be observed in Fig. 6a that the lines at low frequency in the Nyquist plots tend to be more vertical (near 90°) for the capacitor that includes GON independent of the temperature. This may be interpreted as an increase in the capacitance derived from a purely electrostatic double layer, i.e., one in which ionic species have easier access to the carbonaceous surface [19].

Figure 7 shows cyclic voltammograms for the supercapacitors at 25 °C and 100 °C with an electrochemical window of 4 V. Samples exhibit a box-like shape typical of charge storage [25]. The devices present an increase in capacitance of 15 % and 10 % for DWCNT-based electrodes and mixed carbon-based supercapacitors, respectively, as a function of temperature as shown in Table 1. The differences in the capacitance values obtained by voltammetry and impedance spectroscopy, as shown in Table 1, are related to the experimental properties of each technique. Voltammetry is based on a linear sweep of potential. With impedance spectroscopy, an alternating signal is applied, and the phase difference between the applied and measured signal is related to the contributions from different components of the electrochemical cell.

The increase in capacitance as a function of temperature (Table 1) was significantly lower than that obtained in our previous work [32] using a polymer electrolyte and DWCNT–COOH electrode. The polymer electrolyte-based

Table 1 Specific capacitance for two different supercapacitors from distinct electrochemical measurements, at 25 °C and 100 °C

Device electrode	Temperature (°C)	Specific capacitance ($F g^{-1}$)	
		Impedance	Voltammetry (4 V)
DWCNT*	25	26.0	38.2
	100	37.9	43.9
DWCNT*–GON	25	21.7	43.1
	100	39.1	47.6

*Alternated layers of –COOH and –NH2 functionalized DWCNT

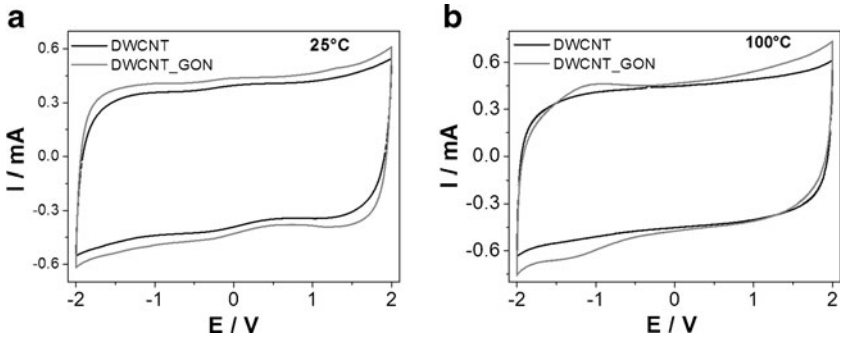

Fig. 7 Cyclic voltammograms for supercapacitors at 100 mV s^{-1} using a potential window of 4 V at temperatures of **a** 25 °C and **b** 100 °C. (DWCNT means layers of alternated functionalized nanotubes)

supercapacitor in the previous work showed a better performance improvement because polymer melting (>40 °C) induces a significant increase in conductivity and electrode wettability. The ionic liquid does not have a thermal transition in the temperature range studied; therefore, the temperature dependence is less significant in the present work.

Hastak et al. [39] recently reported a 26 % increase in the specific capacitance as a function of temperature for a device based on a phosphoric acid electrolyte embedded in a polymer membrane and an activated carbon electrode. They attributed the improvement in the capacitance to the migration of free phosphoric acid to the smaller pores of the carbon interface at higher temperatures. Their result was possible because of the small size of the ionic species involved, which are different than the ionic liquid-based supercapacitors. Pseudo-capacitance at high temperatures also contributed to their results [39].

Capacitance values obtained in this work are similar to those obtained for supercapacitors using ionic liquids as electrolytes that have been reported by other authors [6, 19, 23, 40]. The voltammetric curves obtained at 4-V potential window and 100 °C (Fig. 7b) demonstrate the possibility that the materials employed in the present work could be used ender harsh condition.

Galvanostatic charge–discharge experiments were carried out at 60 °C to evaluate the capacitor´s stability at a typical temperature of use for application in vehicles. A current density of 1 mA cm^{-2} was used, and different potential ranges were studied (0–2 V and 0–3 V). Figure 8 shows the variation in specific capacitance with the number of charge–discharge cycles for both capacitors at a voltage of 2 V. Specific capacitance measured during discharge was calculated by Eq. (1) [41] in which i, Δt, ΔV, and m denote discharge current, discharge time, potential range, and carbon mass in electrode, respectively.

$$C_{sp} = \frac{i\,\Delta t}{\Delta V\, m}$$

The capacitance decayed approximately 30 % after 2,000 cycles for both capacitors operating at 60 °C and at a voltage of 3 V. This is probably associated with irreversible faradic pseudo-capacitance. When the voltage was reduced to 2 V, the capacitance decayed 17 % for DWCNT-based and 10 % for DWCNT_GON-based supercapacitors after 2,000 cycles as shown in Fig. 8.

The charge–discharge results at 2 V also showed higher capacitance values for the mixed carbon nanomaterials-based supercapacitor as previously indicated by the impedance and voltammetry results (Table 1). The two capacitors presented efficiencies of approximately 92 %, indicating a reversibility of charge–discharge cycles. The supercapacitors exhibited energy density values between 3 and 7 Wh kg^{-1}.

Conclusions

The BDIMIM-TFSI ionic liquid exhibited desirable properties for use as a supercapacitor electrolyte, including sufficiently high conductivity (1.65 mS cm^{-1} at 25 °C) and high thermal and electrochemical stability.

Morphological and electrochemical studies of the electrodes developed based on functionalized double-walled carbon nanotubes and the mixture of carbon nanotubes and graphene oxide nanoplatelets showed that both systems can be applied in capacitors. The DWCNT_GON electrodes presented on surface regions with smother graphene

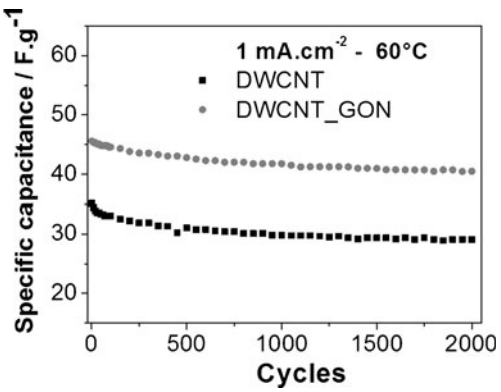

Fig. 8 Change in the specific capacitance as a function of the number of charge–discharge cycles for DWCNT- and DWCNT_GON-based supercapacitors at 2 V and 60 °C. (DWCNT means layers of alternated functionalized nanotubes)

surfaces connecting carbon nanotube globules. A morphology with less packing due to differences in the shapes of the carbonaceous nanomaterials (e.g., nanotubes and platelets) most likely allowed for better wettability of the carbonaceous nanomaterials by the ionic liquid.

The impedance and voltammetry characterization indicated an improvement in the supercapacitor performance with the use of a mixed carbonaceous electrode. An 8 % increase in specific capacitance was observed by voltammetry at 100 °C. The two capacitors were submitted to galvanostatic charge/discharge measurements at 60 °C. These capacitors showed a low capacitance loss after 2,000 cycles, a Coulombic efficiency of 92 %, and an energy density of 7 Wh kg^{-1}, indicating that this configuration can be considered for developing electrochemical capacitors that work safely at high temperatures.

Acknowledgements R.S. Borges acknowledged scholarship from the Brazilian agency CNPq. The authors would like to thank Centro de Microscopia—UFMG for electronic microscopy images.

References

1. Kotz R, Carlen M (2000) Electrochim Acta 45:2483–2498
2. Miller JR, Simon P (2008) Science 321:651–652
3. Zhu Y, Murali S, Stoller MD, Ganesh KJ, Cai W, Ferreira PJ, Pirkkle A, Wallace RM, Cychosz KA, Thommes M, Su D, Stah EA, Ruoff RS (2011) Science 332:1537–1541
4. Miller JR, Outlaw RA, Holloway BC (2010) Science 329:1637–1639
5. Balducci A, Dugas R, Taberna PL, Simon P, Plée D, Mastragostino M, Passerini S (2007) J Power Sources 165:922–927
6. Xu B, Wu F, Chen R, Cao G, Chen S, Wang G, Yang Y (2006) J Power Sources 158:773–778
7. Armand M, Endres F, MacFarlane DR, Ohno H, Scrosati B (2009) Nature Mat 8:621–629
8. Andriyko YO, Reischl W, Nauer GE (2009) J Chem Eng Data 54:855–860
9. Matsumoto K, Hagiwara R (2009) Inorganic Chemistry 48:7350–7358
10. Galinski M, Lewandowski A, Stepniak I (2006) Electrochim Acta 51:5567–5580
11. Bazito FFC, Kawano Y, Torresi RM (2007) Electrochim Acta 52:6427–6437
12. Lewandowski A, Swiderska-Mocek A (2009) J Power Sources 194:601–609
13. Nadherna M, Dominko R, Hanzel D, Reiter J, Gaberscek M (2009) J Electrochem Soc 156:A619–A626
14. Fletcher SI, Sillars FB, Carter RC, Cruden AJ, Mirzaeian M, Hudson NE, Parkinson JA, Hall PJ (2010) J Power Sources 195:7484–7488
15. Borodin O, Gorecki W, Smith GD, Armand M (2010) J Phys Chem B 114:6786–6798
16. O'Mahony AM, Silvester DS, Aldous L, Hardacre C, Compton RG (2008) J Chem Eng Data 53:2884–2891
17. Noked M, Soffer A, Aurbach D (2011) J Sol St Electrochem 15:1563–1578
18. Lavall RL, Borges RS, Calado HDR, Welter C, Trigueiro JPC, Rieumont J, Neves BRA, Silva GG (2008) J Power Sources 177:652–659
19. Liu H, Zhu G (2007) J Power Sources 171:1054–1061
20. Largeot C, Portet C, Chmiola J, Taberna P-L, Gogotsi Y, Simon P (2008) J Am Chem Soc 130:2730–2731
21. Sun G, Li K, Liu Y, Wang J, He H, Wang J, Gu J, Li Y (2011) J Sol St Electrochem 15:607–613
22. Emmenegger C, Mauron P, Sudan P, Wenger P, Hermann V, Gallay R, Zuettel A (2003) J Power Sources 124:321–329
23. Pushparaj VL, Shaijimon MM, Kumar A, Murugesan S, Ci L, Vajtai R, Linhardt RJ, Nalamasu O, Ajayan PM (2007) PNAS 34:13574–13577
24. Portet C, Taberna PL, Simon P, Flahaut E, Laberty-Robert C (2005) Electrochim Acta 50:4174–4181
25. Frackowiak E, Beguin F (2001) Carbon 39:937–950
26. Trigueiro JPC, Borges RS, Lavall RL, Calado HDR, Silva GG (2009) Nano Res 2:733–739
27. Potts JR, Dreyer DR, Bielawski CW, Ruoff RS (2011) Polymer 52:5–25
28. Stoller MD, Park S, Zhu Y, An J, Ruoff RS (2008) Nano Letters 8:3498–3502
29. Wang D-W, Li F, Wu Z-S, Ren W, Cheng H-M (2009) Electrochemistry Communications 11:1729–1732
30. Zhao X, Tian H, Zhu M, Tian K, Wang JJ, Kang F, Outlaw RA (2009) J Power Sources 194:1208–1212
31. Fu C, Kuang Y, Huang Z, Wang X, Yin Y, Chen J, Zhou H (2011) J Sol St Electrochem 15:2581–2585
32. Borges RS, Miquita DR, Silva GG (2011) Electrochmica Acta 56:4650–4656
33. Hummers WS, Offeman RE (1958) J Am Chem Soc 80:1339–1339
34. Guoxiu W, Xiaoping S, Bei W, Jane Y, Jinsoo P (2009) Carbon 47:1359–1364
35. Lee SW, Kim B-S, Chen S, Shao-Horn Y, Hammond PT (2009) J Am Chem Soc 131:671–679
36. Ngo HL, LeCompte K, Hargens L, McEwen AB (2000) Thermochimica Acta 357:97–102
37. Lewandowski A, Galinski M (2004) J Phys Chem Solids 65:281–286
38. Barisci JN, Wallace GG, MacFarlane DR, Baughman RH (2004) Electrochemistry Communications 6:22–27
39. Hastak RS, Sivaraman P, Potphode DD, Shashidhara K, Samui AB (2012) Electrochim Acta 59:296–303
40. Sato T, Masuda G, Takagi K (2004) Electrochim Acta 49:3603–3611
41. Girija TC, Sangaranarayanan MV (2006) Synthetic Metals 156:244–250